J Neuropathol Exp Neurol
Vol. 72, No. 5
May 2013
pp. 416–431

ORIGINAL ARTICLE

Brain Microvascular Accumulation and Distribution of the NOTCH3 Ectodomain and Granular Osmiophilic Material in CADASIL

Yumi Yamamoto, PhD, Lucinda J.L. Craggs, PhD, Atsushi Watanabe, PhD, Trevor Booth, PhD, Johannes Attems, MD, Roger W.C. Low, PhD, Arthur E. Oakley, MIBiol, and Raj N. Kalaria, FRCPath

Abstract

Cerebral autosomal dominant arteriopathy with subcortical infarcts and leukoencephalopathy (CADASIL), the most common form of familial brain arteriopathy, is associated with deposition of granular osmiophilic material (GOM). We used immunohistochemistry and immunogold electron microscopy (EM) to examine the distribution of GOM and NOTCH3 ectodomain (N3ECD) protein in microvasculature of brain gray matter and white matter in patients with CADASIL, non-CADASIL hereditary small-vessel disease and sporadic age-related degenerative disease, and comparable-age controls. We observed intense immunostaining patterns with 2 different anti-N3ECD antibodies in CADASIL but not in young and older controls or other small-vessel disease patients. In addition, CADASIL samples exhibited immunoreactivity in arterial walls and in most capillaries. Electron microscopy revealed profound and widespread extracellular distribution of 0.2- to 2-μm GOM deposits associated with meningeal vessels and perforating arteries and arterioles. Granular osmiophilic material was adjacent to capillaries even within white matter. Immunogold EM with antibody A1-1 to N3ECD revealed abundant particles in GOM within microvessels, vascular smooth muscle cell membranes, and perivascular cells. Granular osmiophilic material did not exhibit immunogold labeling for smooth muscle α-actin or collagen IV. These results showed the specificity of the antibodies and confirm the predominant localization of N3ECD within GOM deposits. The extensive distribution of N3ECD-GOM complexes within meninges, arteries, arterioles, and particularly capillaries in the brains of CADASIL patients suggests that NOTCH3 fragments are major components of GOM deposits, which may be eliminated via perivascular routes.

Key Words: Blood-brain barrier, CADASIL, Electron microscopy, Granular osmiophilic material, NOTCH3, Small-vessel disease, Vascular dementia, White matter.

Centre for Brain Ageing and Vitality, Institute for Ageing and Health, Newcastle University, Campus for Ageing & Vitality, Newcastle upon Tyne, United Kingdom (YY, LJLC, JA, RWCL, AEO, RNK); Department of Surgery and Clinical Science, Yamaguchi University Graduate School of Medicine, Yamaguchi (YY); and Laboratory of Research Advancement, Research Institute, National Center for Geriatrics and Gerontology, 35 Gengo Gengo, Morioka, Obu City (AW), Japan; and Bio-imaging Unit, Newcastle University, Newcastle upon Tyne, United Kingdom (TB).

Send correspondence and reprint requests to: Raj N. Kalaria, MD, PhD, FRCP, Institute for Ageing and Health, Newcastle University, Campus for Ageing & Vitality, Newcastle upon Tyne, NE4 5PL United Kingdom; E-mail: raj.kalaria@ncl.ac.uk

Yumi Yamamoto and Lucinda J.L. Craggs contributed equally to this study and report.

This work is supported by grants from the Newcastle Centre for Brain Ageing and Vitality (BBSRC, EPSRC, ESRC and MRC, LLHW), UK Medical Research Council (MRC, G0500247), an Overseas Research Student Award (YY), and the Alzheimer's Research Trust (UK). Tissue for this study was collected by the Newcastle Brain Tissue Resource, which is funded in part by a grant from the UK MRC (G0400074), by the Newcastle NIHR Biomedical Research Centre in Ageing and Age Related Diseases award to the Newcastle upon Tyne Hospitals NHS Foundation Trust, and by a grant from the Alzheimer's Society and Alzheimer's Research UK as part of the Brains for Dementia Research Project.

The authors have no competing interests to declare.

INTRODUCTION

Cerebral autosomal dominant arteriopathy with subcortical infarcts and leukoencephalopathy (CADASIL) is the most common monogenic hereditary stroke disorder. Mutations in the *NOTCH3* gene segregate with CADASIL. The disease is characterized by multiple small infarcts that are predominantly within subcortical structures, widespread arteriolosclerosis involving vascular smooth muscle cell (VSMC) degeneration, and leukoencephalopathy (1–3). Cerebral autosomal dominant arteriopathy with subcortical infarcts and leukoencephalopathy is distinguished from the other similar hereditary vascular disorders by the unique deposition of granular osmiophilic material (GOM) in systemic and brain vasculature (4–7). Patients with CADASIL may occasionally exhibit brain hemorrhages (8). By light microscopy, GOM deposits are observed as particulate, 1- to 2-μm, periodic acid-Schiff (PAS)–positive granular material. Under electron microscopy (EM), they are detected as electron-dense masses located at intervals around VSMCs (3, 9). Granular osmiophilic material has also been found in capillary basement membranes, where it is frequently associated with pericytes but to a lesser extent than in deposits in arterioles of skin and muscle biopsy specimens (10, 11). The relationship of GOM localization in the vasculature to the pathogenesis of CADASIL is unclear. Similarly, the composition of GOM remains largely unknown.

The NOTCH signaling pathway is thought to undergo a complex series of proteolytic cleavage events, eventually

mediating transcriptional activation of target genes (12). NOTCH receptor ligands such as Jagged and Delta are activated by endocytosis to interact with NOTCH, and the NOTCH ectodomain (NECD) is transendocytosed by the ligand-presenting cell. On further cleavage at sites S2 and S3, an intracellular domain (ICD) is produced that then translocates to the nucleus and binds to the DNA-binding protein CBF1/RBP-Jκ, Suppressor of Hairless and Lag-1 (CSL), to promote transcriptional activity of its target genes such as the hairy/enhancer-of-split (Hes). Joutel and colleagues (13) first described the presence of NOTCH3 ectodomain (N3ECD), but not the ICD in the cerebral vasculature. They indicated that it was located on VSMC plasma membranes in apposition to GOM deposits (13). Using skin biopsy samples, Ishiko et al (14) further demonstrated the immunocytochemical localization of N3ECD within the GOM, but not exclusively on the plasma membrane. Because both previous studies on skin biopsies demonstrated absence of ICD accumulation, N3ECD or GOM secretion or accumulation might occur after the ligand-induced transendocytosis stage of N3ECD production and the subsequent dissociation of ICD. We hypothesize that N3ECD-containing GOM is secreted by VSMC possibly to remove the potentially cytotoxic aggregation-prone mutant N3ECD (15, 16); this may then be eliminated through perivascular drainage routes (17).

Using well-characterized antibodies (12, 18), we examined the specific N3ECD accumulation in relation to GOM in the cerebral vasculature and brain parenchyma of genotyped and clinically characterized CADASIL patients and compared findings with other non-CADASIL hereditary and sporadic small-vessel diseases (SVDs) of the brain. We also investigated VSMC elements and ubiquitin protein in GOM deposits to provide insight into the mechanisms of their formation.

MATERIALS AND METHODS

Subjects and Neuropathologic Examination

Demographic data and relevant genotypes of the 75 patients whose brain autopsy tissue samples were studied are shown in Table 1. To test CADASIL disease specificity, we analyzed brain samples from patients with non-CADASIL hereditary SVDs, vascular dementia characterized by typical SVD (19), Alzheimer disease (AD), cerebral amyloid angiopathy (CAA), and dementia with Lewy bodies (20). The mean ages at death of the CADASIL and any of the control groups were not different ($p > 0.05$). Most of the CADASIL patients had mutations in exon 4 of the *NOTCH3* gene (Table 1). Patients with CADASIL had a strong family history (21, 22) and first experienced stroke-like events between the ages 36 and 50 years (1). They had experienced frequent transient ischemic attacks and multiple cerebral infarcts manifested as sudden onset of weakness, vertigo, and double vision. Where available, magnetic resonance imaging revealed lesions in subcortical regions, brainstem, and basal ganglia and features of cerebral atrophy (21). Most of the patients were abulic and exhibited pseudobulbar, pyramidal, cerebellar, and extrapyramidal signs. Cognitive functions were also diminished in the last year of life, and patients exhibited typical stepwise progression of subcortical-type dementia. Bronchopneumonia was the most common cause of death (21). Most of the CADASIL patients had no history of cardiovascular disease.

The non-CADASIL vascular and neurodegenerative diseases were pathologically diagnosed according to recently established criteria after thorough histopathologic examination of extensively sampled brain sections (9, 23–26). Briefly, hematoxylin and eosin (H&E) staining was used for assessment of structural integrity and infarcts; Nissl and Luxol fast blue staining were used for cellular pattern and myelin loss; Bielschowsky silver impregnation was used for Consortium to Establish a Registry for Alzheimer Disease (CERAD) rating of neuritic plaques; and tau immunohistochemistry was used for Braak staging of neurofibrillary tangles. A diagnosis of AD was made when there was evidence of significant AD-type pathology (Braak stages V–VI and moderate to severe CERAD score) and absence of significant vascular pathology (24). Dementia with Lewy bodies was diagnosed in the presence of significant densities of cortical Lewy bodies and Lewy neurites (25). The diagnosis of SVD form of vascular dementia was made when there were multiple or cystic infarcts, lacunae, microinfarcts and SVD, and Braak stage less than III (23). The degree of CAA was rated as described previously based on a modified version of Vonsattel scoring system (27) and confirmed with immunohistochemistry using antibodies to amyloid β, clone 4G8 at dilution 1:3000 (Senetek, Maryland Heights, MO). Global vascular pathology was assessed as previously described (19), and median vascular pathology scores were calculated as the sum of ratings of vascular pathology in the hippocampus, frontal lobe, temporal lobe, and basal ganglia to generate a score up 10 for this study (19). None of the controls had clinical evidence of neurologic or psychiatric disorder. Neuropathologic examination of brain tissues from controls showed no significant pathologic diagnosis.

Immunohistochemistry

For routine histopathology and screening of NOTCH3 fragment accumulation, we used 10-μm paraffin sections from the gray matter (GM) and white matter (WM) of frontal, parietal, temporal, and occipital lobes. Some sections were also derived from the caudate putamen and cerebellum. Sections were stained with NOTCH3 receptor–related antibodies at different dilutions as follows: anti-N3ECD (A1-1, 1:25,000), anti-N3ECD N1, and anti-ICD C2 (1:1000) (12, 18). Rabbit polyclonal anti-human NOTCH3 antibodies (A1-1, N3ECD N1, and N3ICD C2) were raised against Keyhole Limpet Hemocyanin carrier proteins containing synthetic peptide (amino acid residues 1555–1569; A1-1) or glutathione-S-transferase (GST) fusion proteins containing amino acid residues 42–181 (N1) and 2261–2321 (C2) from the human Notch3, respectively. The specificities of these antibodies were established by immunoblotting (12). To verify the presence of different cellular components of the vasculature, sections were also immunostained with antibodies to smooth muscle α-actin (SMA) at dilution 1:500 (DAKO Cytomation, Glostrup, Denmark), glucose transporter 1 (GLUT-1) at 1:200 (antibody 21041; Thermo Scientific, Middletown, VA), collagen IV at 1:500 (antibody C1926 Sigma, UK), or ubiquitin at dilution 1:50 (DAKO Cytomation).

TABLE 1. Demographic Details of Subjects Screened With A1-1 Antibody for N3ECD Accumulation

	Young Controls	Old Controls	Oldest Old	SVD	CADASIL	PADMAL	Swedish hMID	HERNS	AD	CAA	DLB
n (N = 75)	11	10	4	10	11	5	4	1	7	7	7
Mean age, years	58.1	85.1	101	81.0	59.7	50.0	42.5	39	76.7	83.3	75.4
Range, years	49–69	80–94	96–104	67–96	44–74	41–59	30–48	—	63–87	77–88	71–85
Sex (male/female)	6/5	2/8	1/3	5/5	7/3	2/3	2/2	0/1	3/4	3/4	4/3
Mean age at onset, years	—	—	—	n/a	46.2	40.8	33.8	30	61.5	74.0	69.0
Duration of disease, years	—	—	—	n/a	10.9	11.6	8.6	10	8	10.3	6.6
Gene mutations	—	—	—	—	*NOTCH3*: R133C (2), R141C (3), R153C (2), R169C (3), R558C (1)	—	—	*TREX1* – *3835_3836 insA*	—	—	—
Notable clinical features	—	—		White matter disease, lacunar strokes, dementia	Migraine, TIA, lacunar strokes, dementia	Gait disturbances, emotional disturbances, lacunar strokes, epilepsy in one case, dementia	Gait disturbances, emotional disturbances, lacunar strokes, dementia	Retinopathy, lacunar strokes, cognitive impairment	Memory impairment; dementia	ICH, memory impairment, dementia	Movement disorder, fluctuations, dementia
Cause(s) of death	Cardiac arrest, cancer, renal failure, infection	Heart failure, cancer, ischemic bowel infection.	Cardiac arrest, cancer, renal failure, infection	Heart failure, cancer, GI bleed, sudden death	Bronchopneumonia, heart failure	Pulmonary embolism, heart failure, suicide	Respiratory failure, cerebral hemorrhage, dementia	Urinary tract infection	Bronchopneumonia, COPD, renal failure	Bronchopneumonia, chest infection, sudden death	Bronchopneumonia
Neuropathologic features											
Braak staging	0	0–4	1–3	1–4	0	0	0	0	5–6	5–6	3–4
CERAD score	1	2	1	0–2	0	0	0	0	3	2	3
Median vascular pathology score /10	3	5.5	5	6	8	7	5.5	6	8	8	5
Range	2–6	4–8	4–8	5–7	6–10	6–8	5–9	—	5–10	5–10	5–7

Numbers represent either mean of sample or range. The postmortem interval between death and immersion fixation of tissue ranged from 9 to 96 hours. The length of fixation of tissues before paraffin embedding ranged 1 to 7 months. Control subjects had no distinct disease-related pathologic diagnosis. The CAA cases were of type 2 (CAA moderate, n = 2) and type 1 CAA (CAA severe, n = 5).

AD, Alzheimer disease; COPD, chronic obstructive pulmonary disease; DLB, dementia with Lewy bodies; GI, gastrointestinal; HERNS, hereditary endotheliopathy with retinopathy, nephropathy, and stroke; ICH, intracerebral hemorrhage; PADMAL, pontine autosomal dominant microangiopathy and leukoecephalopathy; Swedish hMID, hereditary multi-infarct dementia of Swedish type; TIA, transient ischemic attack; *TREX1*, 3 prime repair exonuclease 1.

To characterize the distribution of NOTCH3 fragments in each case, we used N3ECD antibodies to score immunoreactivities in different blood vessels (Fig. 1) and brain tissue sections by a semiquantitative scoring system. The N3ECD sections were compared with adjacent sections stained with H&E and PAS, and different intensities were graded as none (–), mild (+), moderate (++), and frequent or abundant (+++) reactivity (Table 2).

Immunofluorescence

Six-micrometer-thick sections were cut from paraffin-embedded brain tissue from the frontal cortical regions (Brodmann areas 8–9) to identify locations of primary antigens with primary and immunofluorescent-conjugated secondary antibodies. Sections underwent heat-mediated antigen retrieval in EDTA buffer, followed by blocking in 10% normal horse serum/PBS for 30 minutes, and incubation with primary antibody overnight at 4°C at dilution as follows: A1-1 at 1:10,000; SMA at 1:500; GLUT-1 at 1:200; and glial fibrillary acidic protein at 1:1000. Sections were washed in PBS and incubated for 45 minutes with one of the following secondary antibodies: goat anti-mouse IgG conjugated DyLight 488 at 1:200 (product no. 35502; Thermo Scientific); goat anti-rabbit IgG conjugated DyLight 550 at 1:200 (product no. 84541; Thermo Scientific); and donkey anti-goat Alexa Fluor 350 (product no. 1084434; Life Technologies) at 1:500. Sections were then washed in PBS before mounting in Vectashield (Vector Laboratories, Burlingame, CA). Collagen was immunolocalized with an additional antigen retrieval step. This involved heat-mediated antigen retrieval in EDTA first and then protease digestion 0.033 mg/mL (Subtilisin A type VIII, Sigma), followed by washing in PBS and blocking in 10% horse serum. Sections were then incubated overnight at 4°C with the anti–collagen IV antibody at 1:500 dilution.

Immunoelectron Microscopy

Brain tissues from CADASIL patients and normal controls (Tables 1, 2) were sampled from the GM and WM in frontal and temporal lobes and the cerebral meninges. They were fixed 16 hours in 2% paraformaldehyde and 0.05% glutaraldehyde in 0.1 mol/L phosphate buffer, pH 7.4), then rinsed in 2 changes of PBS. Half of each batch of samples was treated with 1% OsO4 in 0.1 mol/L phosphate buffer. Samples were dehydrated in increasing concentrations of alcohol, cleared in propylene oxide, and then embedded in epoxy resin.

Sections were cut into 1-μm-thick sections using an ultracut microtome (Reichert-Jung, Depew, NY) and stained with 1% toluidine blue and 1% borax to confirm the position of blood vessels in the sections. Ultrathin sections were cut using a DDK Delaware diamond knife and placed onto 3.05-mm nickel 300-square-mesh grids that had been pretreated with 10% nitric acid. Sections that were OsO4 treated were used for morphologic examination, and non–OsO4-treated sections were further processed for immunogold labeling.

Throughout the immunogold staining procedures, Tris buffered saline (pH 7.4) containing 1% bovine serum albumin and 0.1% Tween-20 was used as a buffer. The non-OsO4 epoxy-resin sections were etched with 2 changes of 3% sodium

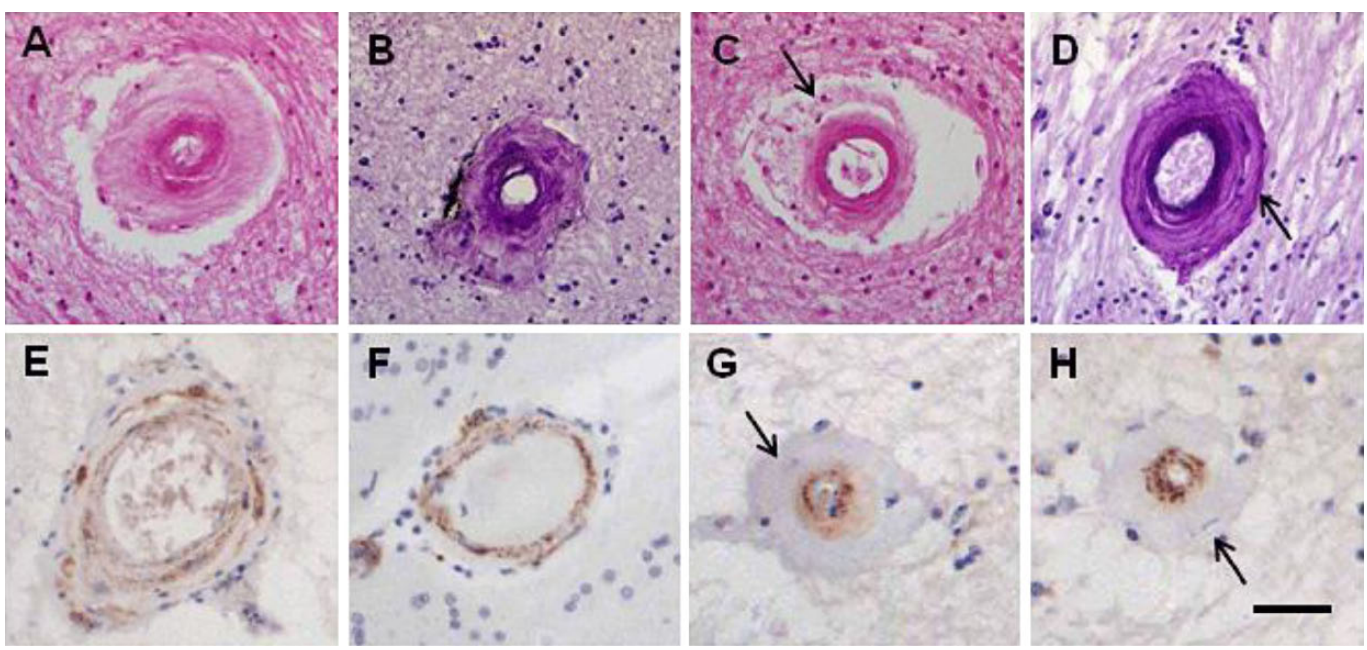

FIGURE 1. Arteriolosclerosis, differential hyalinization, and immunoreactivities of N3ECD in cerebral arterioles in temporal lobe white matter of CADASIL patients. **(A–D)** Arterioles stained with H&E **(A, C)** and PAS **(B, D)** stains show basophilic material and variable degrees of hyalinization (arrows). **(E–G)** Arterioles stained with A1-1 antibody to N3ECD and hematoxylin counterstain in adjacent sections. **(E, F)** Partially and nonhyalinized vessels that contain smooth muscle cells delineated by A1-1 staining and nuclear hematoxylin staining. **(G, H)** Hyalinized vessels with residual perilumen A1-1 staining that are devoid of smooth muscle cell A1-1 and nuclear staining in peripheral hyalinized areas (arrows). Scale bar = 35 μm.

TABLE 2. Distribution of N3ECD Immunoreactivity in CADASIL Patients and Young and Old Controls

		Immunohistochemistry With A1-1 Antibody to N3ECD				Immunoflourescence With A1-1 Antibody to N3ECD	
		Distribution in Vascular Profiles†		Other Comments		Distribution in Vascular Profiles	
Case (n)	Age, years	Arteries	Arterioles	Capillaries	Perivascular Cells	Arterioles	Capillaries
CADASIL (11)	Mean = 60	Yes (7)/No (4)					
CAD1	44	+++	+++	+++	Yes	+++	+++
CAD2	52	++	++	+	Yes	+	+
CAD3	53	++	++	++	Yes	+++	+++
CAD4	55	++	++	–	No	++	+
CAD6	59	+++	+++	++	No	+++	+++
CAD7	61	+++	+++	+++	Yes	+++	+++
CAD8	63	++	+	+/–	No	+	+
CAD9	65	+	+	–	No	+	+
CAD11	68	+++	+++	++	Yes	+++	+++
CAD12	68	+++	+++	++	Yes	+++	+++
CAD13	74	+++	+++	+++	Yes	nd	nd
Ycont (8)*	Mean = 58	–	–	–	Yes (4)/No (4)	–	–
Ocont (7)*	Mean = 75	–	–	–	Yes (5)/No (2)	–	–
OOcont (6)*	Mean = 97	–	–	–	Yes (6)/No (0)	–	–

Score symbols show no (-), mild (+), moderate (++), and frequent/abundant (+++) immunoreactivity. Only CADASIL cases exhibited extensive vascular immunoreactivity.

*A few A1-1–stained capillaries were present in 2 of the oldest control (non-CADASIL) cases. N3ECD immunoreactivity in vascular dementia (VaD) and Alzheimer disease cases was rare. Immunoreactive perivascular cells were also more common in older cases.

†Because most of the microvessels in controls (or VaD) subjects were not stained by A1-1 or N1 antibodies, only the summary scores are shown. Cases CAD6, CAD7, and CAD11 were used for EM studies.

nd, not determined; OCont, old age control; OOCont, oldest old control; YCont, young control.

meta-periodate for 20 minutes and heated in 0.01 mol/L citrate buffer (pH 6) at 90°C for 10 minutes. After blocking with 5% bovine serum albumin, 5% normal goat serum, and 0.1% gelatine in Tris buffered saline, the grids were incubated in N3ECD A1-1 (1:4000), anti-ubiquitin (1:50), anti-SMA (1:100), and anti–collagen IV (1:30; Abcam, Cambridge, MA) diluted in buffer. They were rinsed and subsequently incubated in EM-grade goat anti-rabbit IgG 5-nm gold probes (1:30; BB International, Madison, WI). To increase the visibility of the gold particles, the sections were further treated with a Silver Enhancing Kit for Light and Electron Microscopy (BB International). Sections were postfixed in 2% buffered glutaraldehyde and contrasted with uranyl acetate and lead citrate. Electron microscopy images were taken using a Philips 201 transmission electron microscope coupled to a Gatan multiscan camera, model 791 (Gatan, Pleasanton, CA).

RESULTS

Light Microscopy and N3ECD Accumulation in CADASIL Cerebral Vasculature

At the light microscopic level, H&E and PAS stains demonstrated characteristic basophilic staining, revealing deposition of nonfibrillar amorphous granular material (0.2- to 2-μm size) in the tunica media of numerous arteries and arterioles of both the cortical and subcortical GM and WM (Fig. 1). Using conventional immunohistochemistry, both the antibodies to N3ECD, N1, and A1-1 showed nearly identical but characteristic immunoreactivity in arteries and arterioles in the GM and WM in CADASIL cases (Fig. 2; Table 2). Capillaries were also widely reactive, as confirmed by microvessel size and lack of SMA staining. The most distinctive reactivity was evident in the GM as discontinuous granular staining along the walls of capillaries and sometimes within perivascular cells (Fig. 2C inset). Highly hyalinized vessels did not exhibit N3ECD immunoreactivity within the walls; it was largely restricted to the endothelium (Fig. 1G, H). Only 2 of the oldest old controls had some positive immunostaining around capillaries similar to that seen in CADASIL patients (Fig. 2E, F). Sporadic SVD cases were never positive for N3ECD. Vessels positive for N3ECD were also not evident in the AD or CAA samples. Immunostaining analysis showed that there were no readily observable differences in the vascular immunoreactivity of the C2 antibody (to the ICD) between CADASIL and control samples.

To enable more finite visualization and verify specificity, we used immunofluorescence methods to examine the distribution of N3ECD with the A1-1 antibody in cognitively normal controls, hereditary SVDs, and other common dementing disorders, including AD, CAA, and dementia with Lewy bodies (Table 1). NOTCH3 ectodomain immunoreactivity was mostly observed as punctate or granular deposits within the medial layers of arteries and arterioles and on the surface of the meninges, but venules were rarely reactive (Fig. 3). As before, N3ECD immunoreactivity appeared to bound or ''wrapped'' around basement membranes of almost all capillaries (Fig. 3). This was confirmed by the absence of SMA reactivity and the presence of collagen IV or the endothelial marker GLUT1. There was a slight predominance of

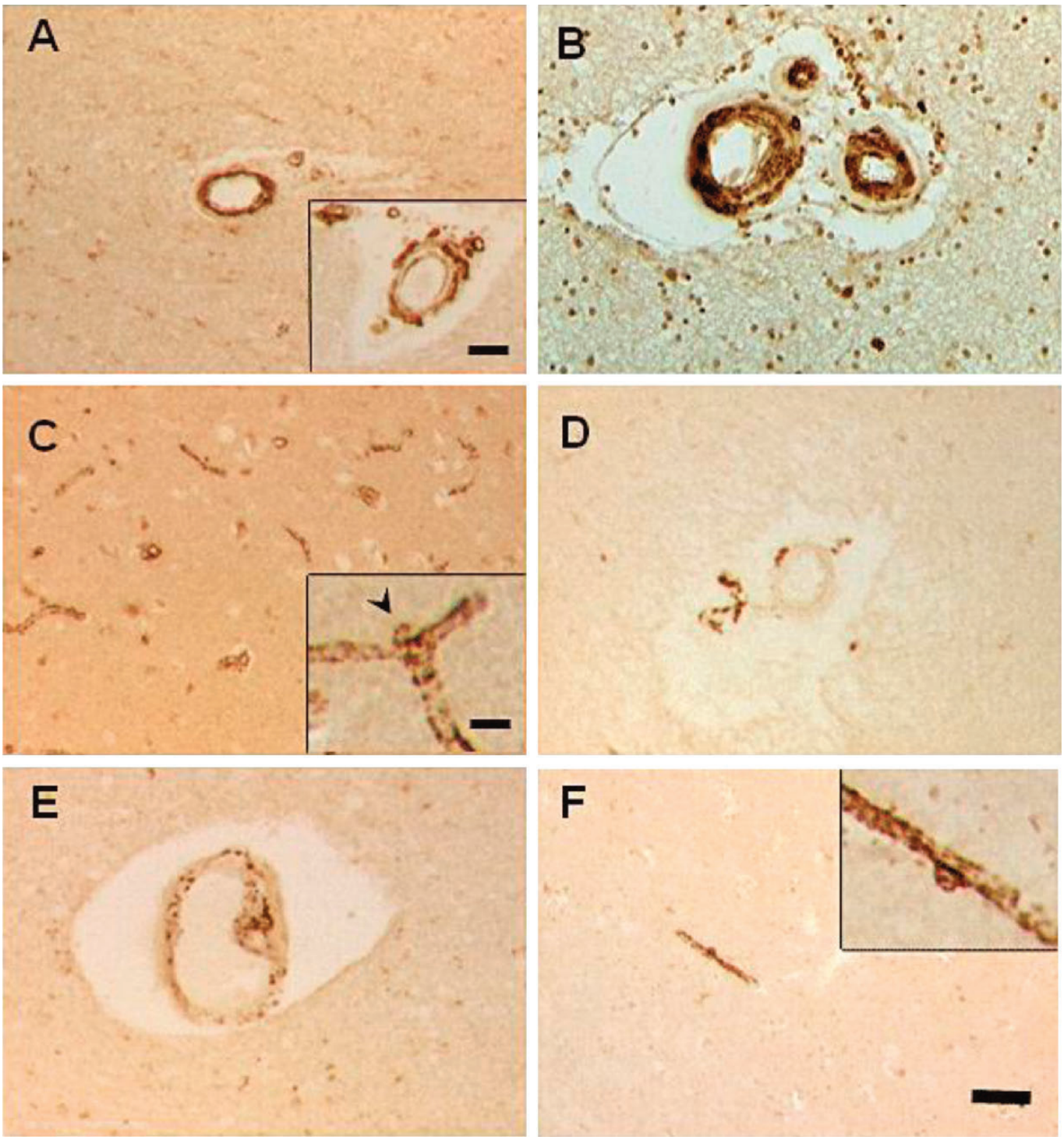

FIGURE 2. Immunohistochemical localization of N3ECD in brains from CADASIL patients and normal control subjects. Large arterioles in white matter **(A, B)** and capillaries in gray matter **(C)** of CADASIL cases were strongly stained with A1-1 **(A, C)** and N1 **(B)** antibodies to N3ECD. Note the granular/punctate deposits in the vessel wall in inset **(A)**. Staining in capillaries is often granular with immunoreactive perivascular cells **([C]** inset, arrowhead**)**. **(D, E)** Vessels of non-CADASIL controls were mostly negative for N3ECD. In some cases, perivascular macrophage-like cells were partially immunoreactive in small vessels **([D]** from a young control; **[E]** from an older control**)**. **(F)** Capillaries in an oldest old control occasionally showed similar immunoreactivity to those in CADASIL. Scale bars = **(A–F)** 50 μm; (inset **A**) 50 μm; **(**inset **C)** 20 μm.

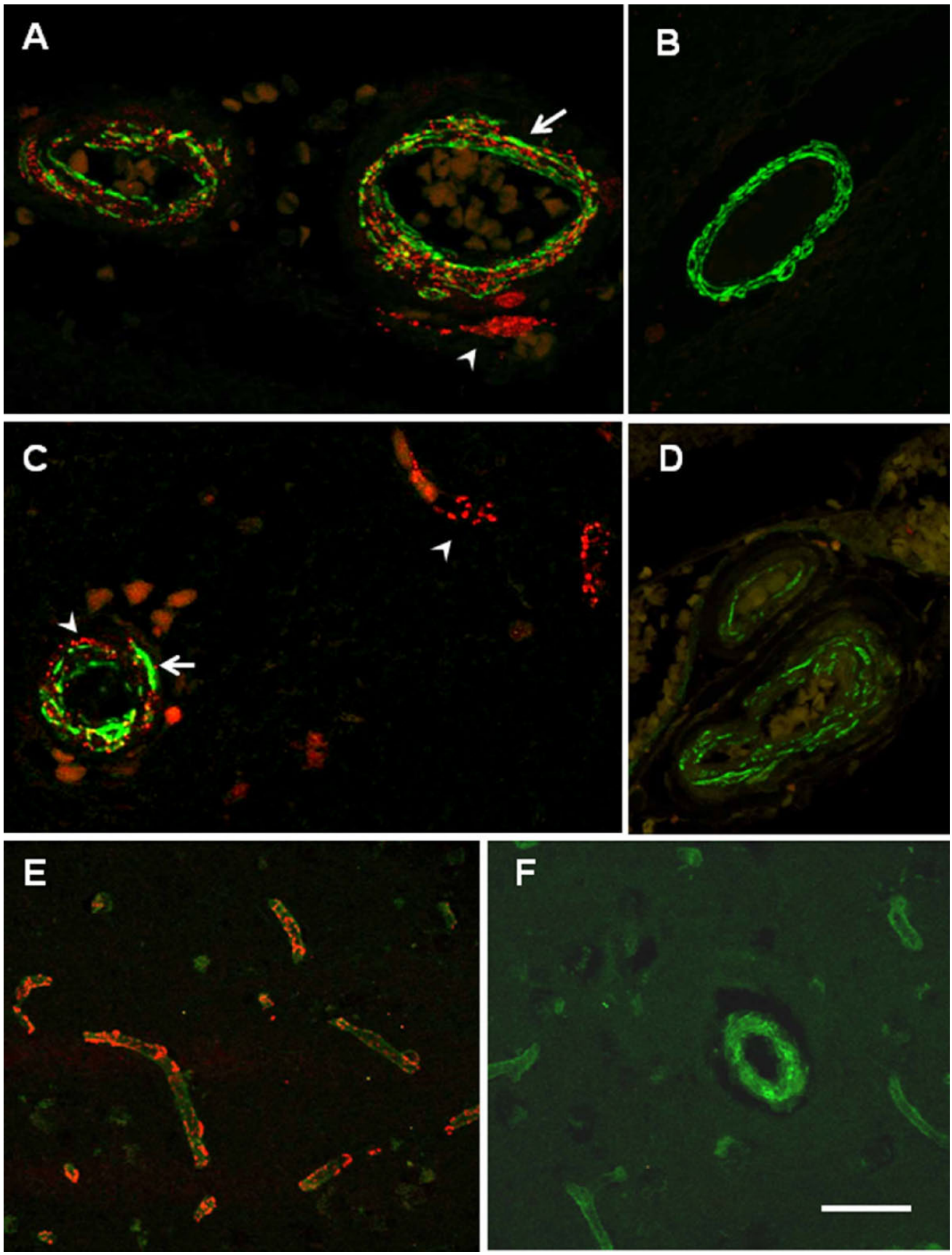

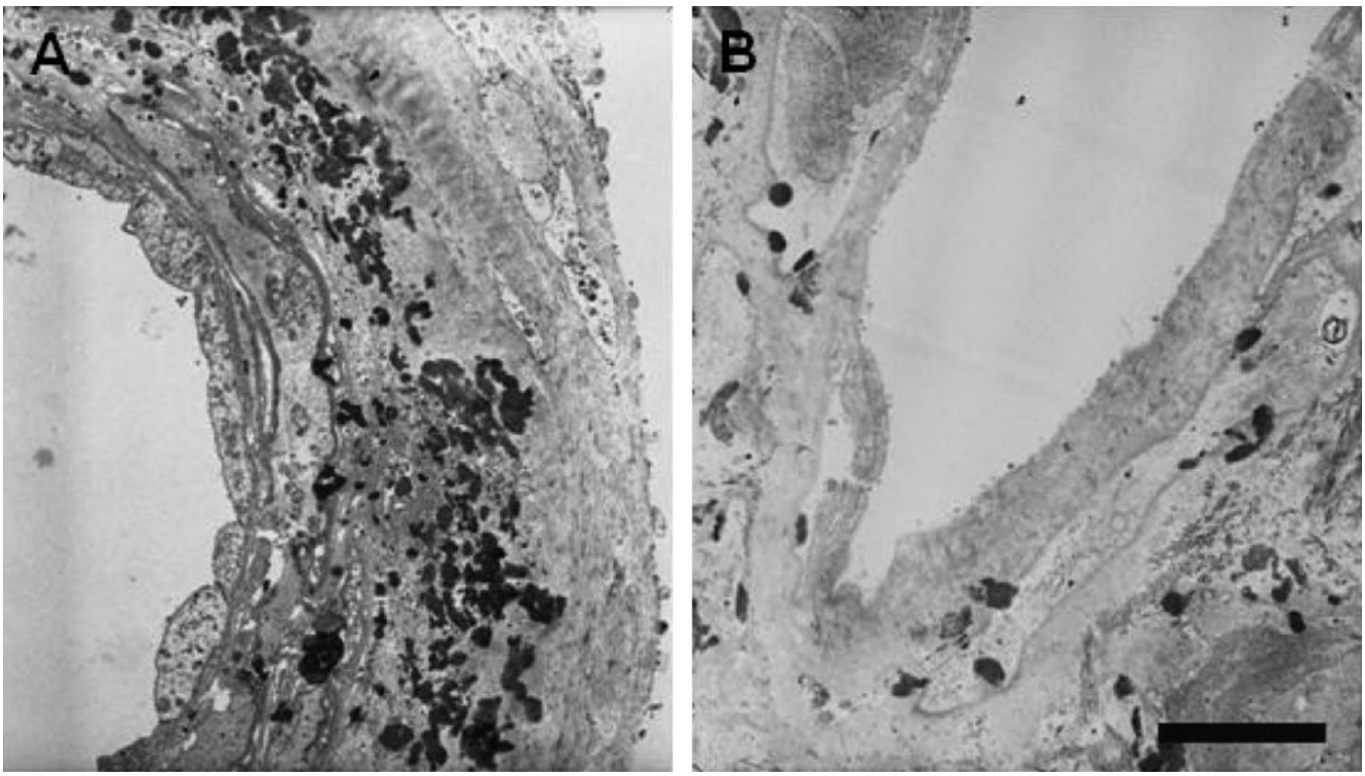

FIGURE 4. Distribution of GOM accumulation in cerebral vessels by electron microscopy in a patient with CADASIL. **(A, B)** Note the large amounts of 0.2- to 2-μm GOM deposits distributed in the meningeal artery **(A)**, not necessarily restricted around VSMCs. The microvessel **(B)** in temporal cortex has smaller amounts of GOM that are in close proximity to VSMCs. The extent of GOM deposits in this case (CAD7) is evident because of high contrast and good morphology. Scale bars = **(A)** 6 μm; **(B)** 4 μm.

N3ECD immunoreactivity in WM compared with GM vessels. Overall, these observations indicate that N3ECD immunoreactivity was specific to CADASIL and only associated with the meninges, arteries, arterioles, and capillaries in CADASIL versus similar age or older controls and the other cases. Based on the semiquantitative distribution data generated both by immunohistochemistry and immunofluorescence methods, N3ECD reactivity was highly specific for CADASIL compared with the relevant controls.

Ultrastructural Localization and Distribution of GOM

We confirmed the light microscopic findings by EM examination of tissues from the GM and WM from 3 CADASIL cases and 1 normal control (Table 2). There was intense and widespread extracellular distribution of GOM deposits associated with meningeal, pial, and perforating arteries and arterioles (Fig. 4). Granular osmiophilic material was also evident adjacent to capillary walls (basement membrane) within the WM, but similar N3ECD immunoreactivity was not apparent in the parenchyma, neurons, axons, or astrocytes.

Distribution of N3ECD in GOM

The GM, WM, and meningeal samples from a 68-year-old CADASIL patient were further processed for immunogold EM. Examination of 1-μm epoxy-embedded tissue sections by light microscopy revealed severe tissue disruption possibly because of extensive trauma suffered by the patient before death. At the EM level, while cellular components such as mitochondria, Golgi apparatus, and endoplasmic reticulum were severely damaged in the GM and WM, the structural components of meningeal arteries were reasonably preserved. Abundant 0.2- to 2-μm GOM deposits were strongly immunoreactive to N3ECD A1-1 antibody observed as immunogold particles (Figs. 5, 6). Granular osmiophilic material containing N3ECD were found not only around VSMCs in arteries and arterioles

FIGURE 3. Immunofluorescence with confocal microscopy demonstrating distribution of N3ECD deposits in brains from CADASIL but not in similar-age control and hereditary multi-infarct dementia (hMID) of Swedish-type patients. **(A–F)** There are widespread punctate or granular deposits of N3ECD (red) in walls of arterioles (smooth muscle α-actin [SMA] positive, green, open arrows) and most capillaries **(A, C, E)**. Deposits of N3ECD (red, arrowheads) can also be seen in the meninges in CADASIL **(A)**. Vessels in young controls **(B, F)** and Swedish hMID **(D)** patients were completely negative for N3ECD. Note the disrupted arterial walls labeled with SMA in CADASIL **(A, C)** and Swedish hMID **(D)** cases. **(A–D)** Stained with antibodies to N3ECD (red) and SMA (green); **(E, F)** stained with antibodies to N3ECD (red) and collagen IV (green). Scale bars = **(A, B, D–F)** 50 μm; **(C)** 20 μm.

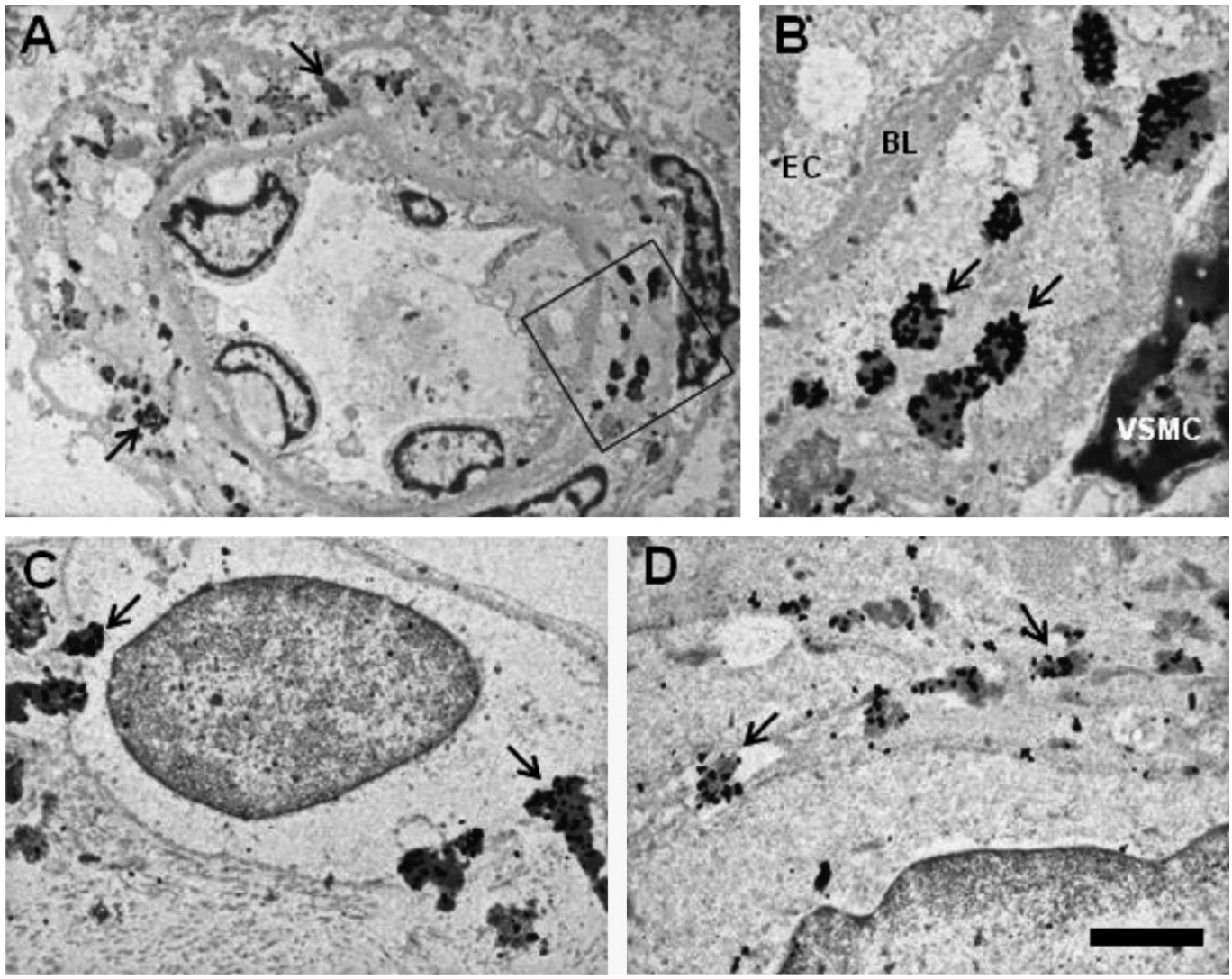

FIGURE 5. Granular osmiophilic material deposits labeled with N3ECD in pial arterioles and capillaries. **(A, B)** Abundant 5-nm gold particles representing N3ECD immunoreactivity in a cortical vessel are in GOM deposits in the tunica media, associated with basement membranes and in close proximity to VSMCs. Box in **(A)** delineates the area shown in **(B)**. **(C, D)** Heterogeneous nature of GOM deposits; the farther from the plasma membrane, the more loosely the granules are associated. The meningeal capillary wall contains abundant GOM deposits that seem freely packed at the outer side of the wall. There is an occasional linear labeling pattern within the cytoplasm (arrows), presumably a phagocytic cell that resembles a mesothelial lining cell **(D)**. Arrows denote areas of N3ECD stained GOM. BL, basal lamina; EC, endothelial cell. Scale bars = **(A)** 3.5 μm; **(B)** 1.5 μm; **(C)** 2μm; **(D)** 1 μm.

but also within basement membrane or around pericytes in the capillaries from GM (Fig. 5). The granular components of GOM were more loosely associated further from the plasma membrane of VSMCs, suggesting that they were dispersed into the interstitial fluid (ISF) (Fig. 6B, C inset). Similarly, the distribution of N3ECD immunoreactivity was uneven within GOM, with more gold particles attached to the higher electron-dense areas. Linearly arranged intracellular gold particle labeling was occasionally observed in several meningeal arterial VSMCs. Clusters of gold particles were only found on the plasma membrane in association with GOM deposits.

We also observed numerous mononuclear cells that seemed to be engulfing GOM deposits within vessel walls (Fig. 7). These cells showed lipid bilayer formation around the GOM on the cell surface (Fig. 7B). Some perivascular cells also contained 0.1- to 0.3-μm inclusion bodies distributed throughout the cytoplasm, some of which were opaque whereas others were more electron dense. A few gold particles were associated with the darkly stained vesicles in these cells, whereas almost none were found in the cytoplasm (Fig. 7C).

No colabeling of GOM deposits was observed in negative controls or when the sections were immunostained with conjugated gold particles or using antibodies to SMA or collagen IV followed by EM (Fig. 8). These observations confirm specific localization of N3ECD but not SMA or collagen IV immunoreactivity within GOM deposits.

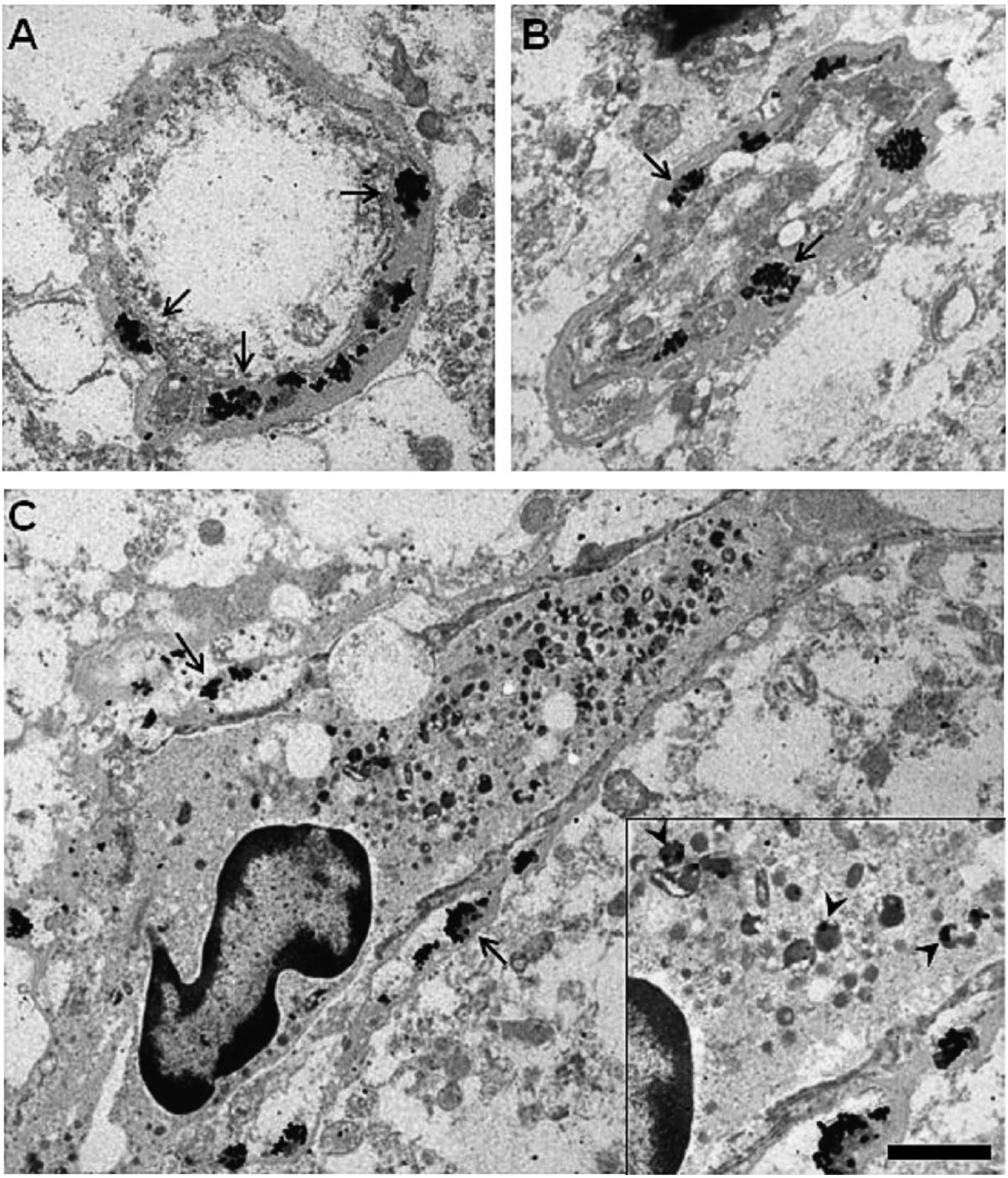

FIGURE 6. Granular osmiophilic material deposits labeled with N3ECD in small vessels and capillaries of cortical gray matter and white matter. **(A–C)** N3ECD-labeled GOM deposits are frequently seen in the capillary basement membranes (identified by lack of VSMCs and size) **(A, B)** and also around perivascular cells, which appeared phagocytic with distinct nucleus **(C)**. A few gold particles were also associated with some of the vesicle-like structures **(**arrowheads in inset **[C])**. Scale bars = **(A, B)** 1.5 μm; **(C)** 2 μm; (**inset**) 1 μm.

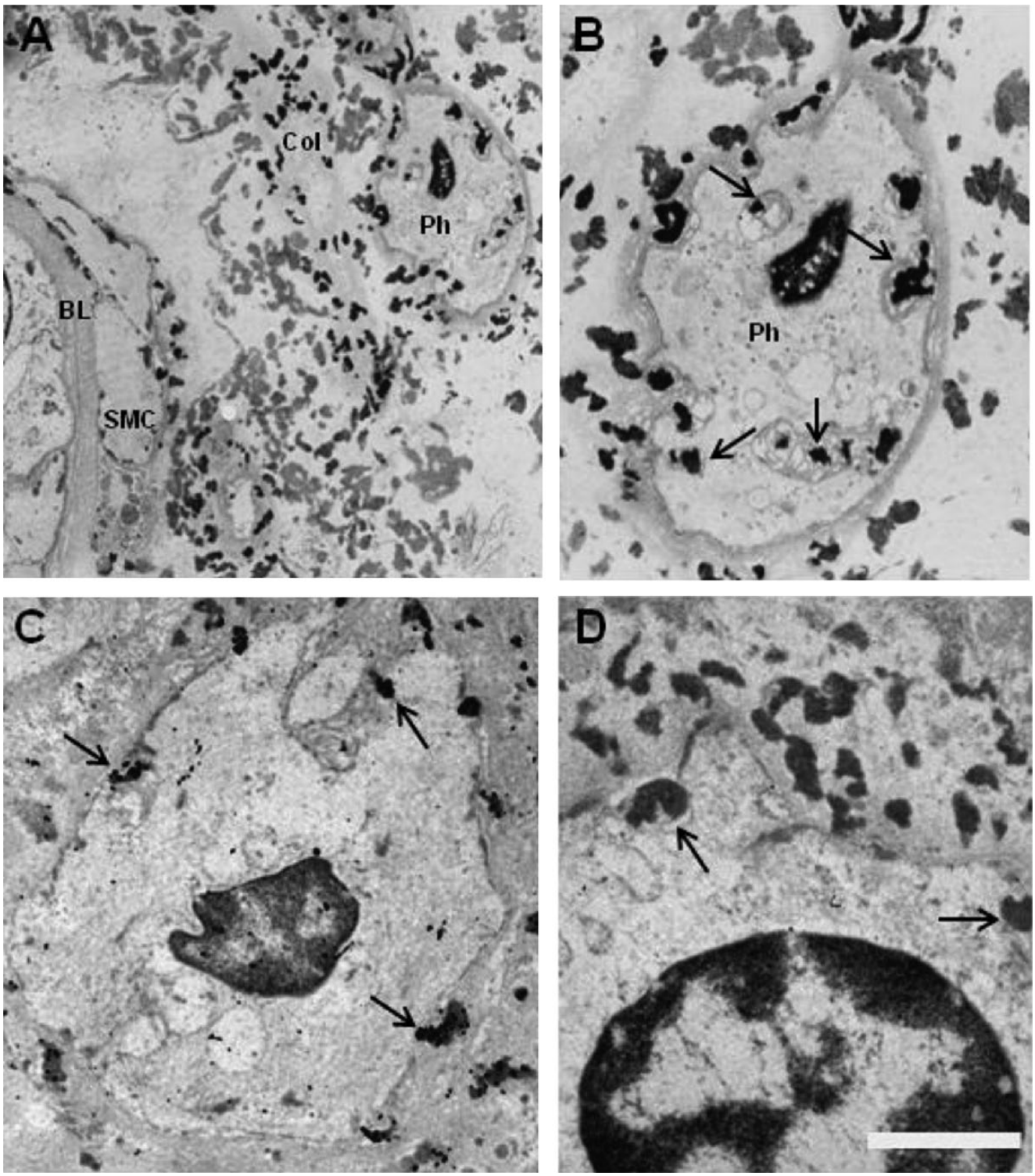

FIGURE 7. Localization of GOM deposits within or being engulfed by perivascular cells. **(A, B)** Numerous GOM deposits are close to degenerated VSMCs and basement membranes **(A)**. The phagocyte-appearing cell (Ph) nearby appears to be engorging or excreting GOM deposits of various sizes in the surrounding area **(B)**. Note the bilayer membrane formation around the GOM with the cell (arrows). **(C)** Another phagocyte-appearing cell engulfs GOM deposits labeled with immunogold N3ECD particles. **(D)** Immunogold-labeled N3ECD in GOM deposits within the border of a mononuclear cell. Arrows denote GOM, either having been internalized into the cell or in the process of being ingested. Note that a dual membrane appears to protect the cell from engulfed toxic substances, possibly indicating a phagocytic protective mechanism. Images are from cases CAD 7 and CAD 11 (Table 2). BL, basal lamina; Col, Collagen layer; SMC, smooth muscle cell. Scale bars = **(A)** 4 μm; **(B, C)** 2 μm; **(D)** 1.5 μm.

Distribution of Ubiquitin in CADASIL

Previous light microscopic observations have revealed ubiquitin immunoreactivity in the tunica media of arterioles in CADASIL. Similar VSMC layer staining was seen in controls but was limited to few arterioles. Capillaries were rarely immunoreactive for ubiquitin in CADASIL or in control cases. Some perivascular cells, possibly macrophages, were strongly stained for ubiquitin (7, 18). To determine whether ubiquitin is localized within GOM, we immunostained ultrathin sections with antibodies to ubiquitin but observed a lack of gold particles linked to ubiquitin specifically overlaid on or attached to GOM (Fig. 8).

DISCUSSION

The present study demonstrates 2 observations pertinent to the pathogenesis of CADASIL. First, we show widespread accumulation and distribution of ectodomain of NOTCH3 in the meninges and the brain microvasculature, particularly capillaries in CADASIL patients. Second, we provide confirmatory EM evidence for the localization of N3ECD within GOM deposits. Granular osmiophilic material deposits were found in close proximity to not only VSMC but throughout the cerebral arterial tree and capillaries. Together, these observations suggest that N3ECD-GOM complexes are widely evident and abundantly produced specifically within the brains of CADASIL patients and appear predominantly along capillaries and perivascular drainage routes (17). Several previous reports have described the distribution of GOM deposits in systemic organ tissues. Our results are consistent with these observations in skin biopsies (10, 11, 28), but GOM deposits appear much more abundant in the brain.

The identity of GOM has been a key question in elucidating CADASIL pathogenesis. Because no study has followed to confirm or refute either of the previous observations on N3ECD localization (13, 14), we examined the presence of N3ECD in GOM deposits with modified EM methods in postmortem human brain tissues. Using terminal-specific antibodies, we demonstrate unequivocally that N3ECD accumulates within GOM deposits located in the meninges and in the tunica media and the basement membrane of arteries, arterioles, and capillaries in both the GM and WM. The slight differences between our observations and previous studies may be attributed to the methodology used to demonstrate GOM localization. The use of pre-embedding method on paraffin-embedded postmortem brain tissues fixed in buffered formalin would not be ideal (13). The method greatly limits the accessibility of antibody to the antigen and reduces antigenicity, which might explain partial immunoreactivity adjacent to GOM (14). On the other hand, Ishiko et al (14) used skin biopsy samples prepared using cryofixation and freeze substitution, which require several tissue-embedding processes at −60°C to −80°C but preserves antigenicity. We sought an easier method that could be used on brain tissues fixed in paraformaldehyde at room temperature, thereby avoiding a false-negative result, that is, the postembedding immunogold staining method. Our approach seems to have maximized the immunoreactivity by the combination of double etching and antigen retrieval in citrate buffer while reducing nonspecific background staining, as demonstrated by the lack of staining in GOM in negative controls and anti–collagen IV–stained sections. The heterogeneous distribution of N3ECD through oligomerization mediated by disulfide bonds (15) suggested the presence of other components. We did not observe the localization of SMA or collagen IV within the GOM-N3ECD complexes. We have not thoroughly tested for the presence of Delta/Serrate/LAG-2 family ligands or non-Delta/Serrate/LAG-2 ligands such as Y-box protein-1, but our preliminary observations suggest absence of JAG-1, DLL1, and DLL4 in GOM deposits (unpublished data). Other ligands should also be tested because it has been suggested that *NOTCH3* mutations alter Fringe glycosylation, which determines ligand preference of the receptor (29, 30). We also did not find ubiquitin immunoreactivity within GOM, although it was present in degenerated VSMC, as expected (18, 31). This does not exclude the possibility that other proteins (e.g. endostatin, clusterin) or cofactors are entrapped in the structure, which may prevent extreme multimerization of mutant N3ECD (16).

Our observations do not indicate whether GOM is directly toxic to vascular or neuronal cells. However, as indicated in transgenic mouse models (32, 33), it is possible that GOM deposits are the result of degeneration rather an instigator of a toxic action. In a previous study, the amount of GOM did not necessarily correlate with VSMC degeneration (32), but, consistent with our EM observations, it was noted that vascular morphologic changes, such as increased intracellular dense bodies, wider intra–smooth muscle and subendothelial spaces, and cellular deformation, preceded the appearance of GOM.

Another intriguing observation in our study was the intracellular immunoreactivity in cells, that is, linear localization of gold probes in VSMCs and in some instances more than 15 isolated N3ECD-labeled gold probes in vesicles within the cytoplasm. It is possible that these represent early formation of aggregates with the Golgi in VSMC or those being metabolized in phagocytic cells. Based on their morphology, these vesicles are presumed to be endosomes or secondary lysosomes, but their origin is difficult to ascertain. There are 2 possible sources of N3ECD in those endosomes: either endogenous or exogenous. Surface expression of NOTCH3 receptor is regulated by its endocytosis from plasma membrane (34) and the recycling or lysosomal degradation that follows. Localization in VSMCs may be consistent with the gain-of-toxic-function or endoplasmic stress hypothesis implicated from cell culture studies (18). However, these observations should be interpreted with caution because several factors inclusive of advanced state of disease, agonal state, extensive postmortem delay, and immersion fixation could have affected the tissue, which had clearly lost much of its morphologic integrity, but the vasculature appeared to be reasonably preserved and membrane-like structures were evident.

We frequently observed phagocytic or scavenging activity whereby macrophage-type cells seemed to be engulfing GOM deposits. We reason that, in the meninges, these represent free mononuclear phagocytic cells derived from clasmatocytes or cells that have ''broken off'' or detached

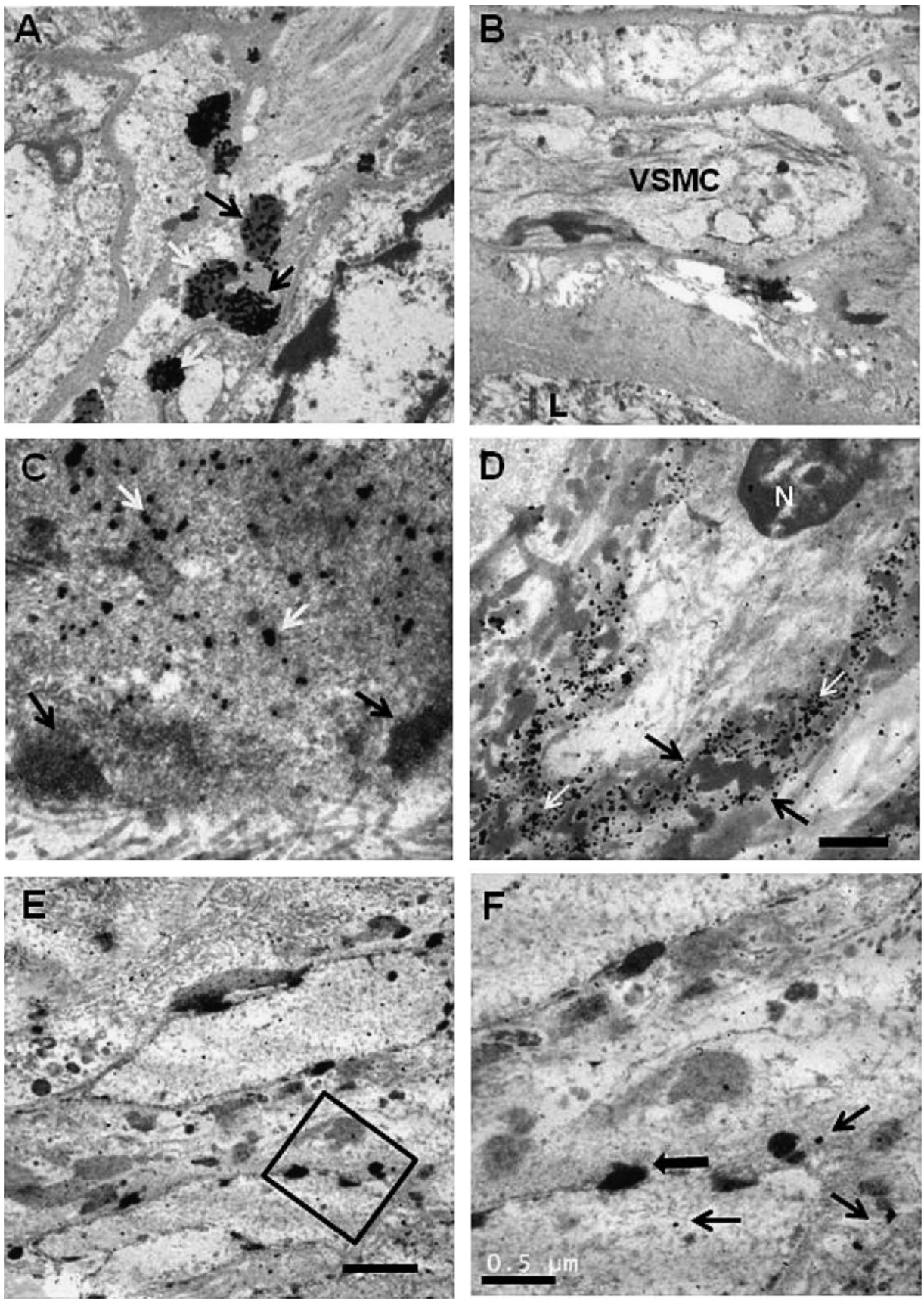

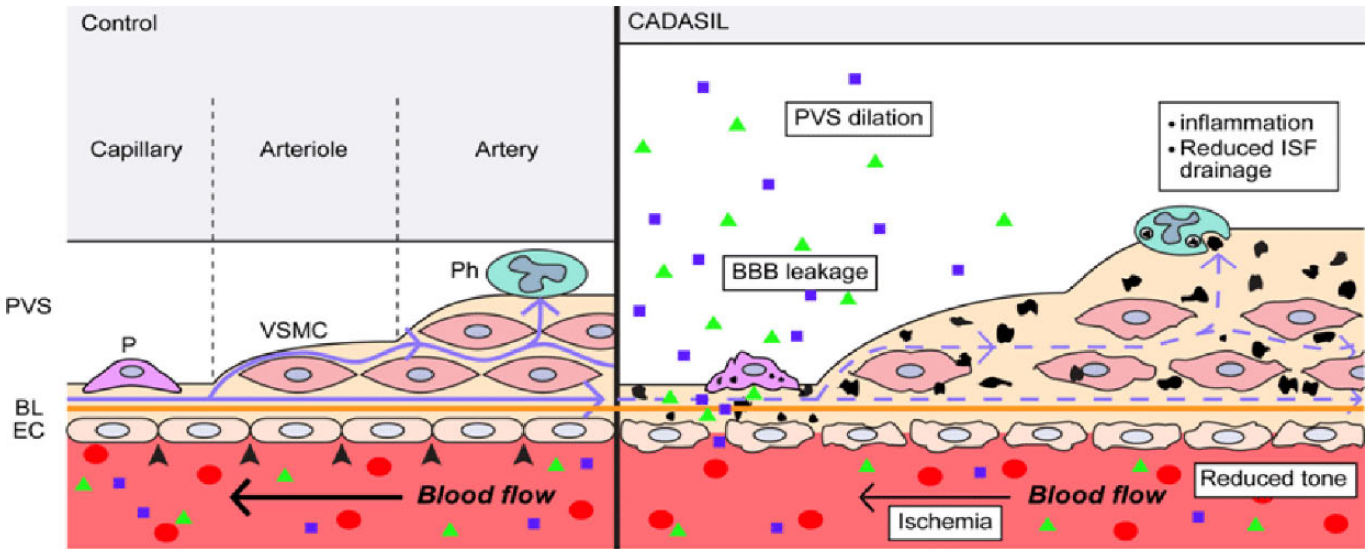

FIGURE 9. Hypothetical scheme showing pathogenetic mechanisms in CADASIL. In normal (control) individuals, tight junctions (arrowheads) between endothelial cells (ECs) sitting on the basal lamina (BL) form the blood-brain barrier (BBB) that protects the brain from cytotoxic substances. Solutes in the ISF drain out of the brain through perivascular drainage pathways driven by vascular pulsation. In CADASIL, there are several changes to the surface between blood and brain parenchyma or CSF at the artery, arteriole, and capillary levels. Most prominently, the arterial wall disintegrates, specifically by VSMC degeneration, EC damage, and enhancement of GOM deposition (black amorphous blobs). These changes may collectively breach the BBB (triangles and squares) and cause injury to perivascular cells (P). The degeneration of VSMC likely reduces vascular tone such that the perivascular drainage of ISF with GOM and other proteins is impeded; this contributes to enlargement of the perivascular space (PVS) and activation of an inflammatory response by macrophages or phagocytic cells (Ph).

from the activated leptomeningeal endothelial cells that normally line the pia and arachnoid mater or possibly from mesothelial lining cells (35). Recent observations suggest that detached leptomeningeal cells with presumptive phagocytic properties release proinflammatory cytokines that activate both microglia and astrocytes during systemic inflammation (36, 37). It is also likely that N3ECD fragments are in vesicles within pericytes (28). Pericytes are known to have not only vasoconstrictive abilities similar to VSMCs but also macrophage-like properties, that is, phagocytosis and pinocytosis, and the capacity to act as initiators of inflammatory responses (38, 39). Our observations may not only implicate natural elimination activity by macrophages/microglia but also the involvement of inflammatory/immune responses in CADASIL. Abnormal deposition of proteins, such as mutant N3ECD-containing GOM in arteries, arterioles, and capillaries, might activate the immune system and cause a chronic inflammatory state (40, 41).

Based on our overall observations, we have formulated a hypothetical perspective to understand the pathogenesis of CADASIL (Fig. 9). The integrity of the blood-brain barrier and clearance of abundant GOM deposits, which may be efficient in younger subjects, are obviously important factors in the pathogenesis of CADASIL and AD. Three major clearance mechanisms for amyloid β deposits have been proposed for AD, but, in contrast to fibrillary β-amyloid deposits, mutant N3ECD is confined to relatively large (0.2–2 μm) granular formations (GOM) without forming any clearly distinguishable structures. Smaller GOM particles appeared to be partly dispersed in ISF, indicating they are not rigid structures. As previously reasoned, the elimination mechanisms of certain proteins such as amyloid β may include protease degradation in the parenchyma, transfer into blood by low-density lipoprotein receptor–related protein 1, and perivascular drainage (42). Whereas the apparent scavenging activity by perivascular cells represents a removal mechanism as discussed above and it is unlikely that relatively large GOM deposits are transported into blood via specific receptors such as the low-density lipoprotein receptor–related protein 1, the clearance of GOM within the ISF through the lymphatic drainage route driven by vascular pulsation (17) seems relevant to CADASIL. Degeneration of VSMC and the accumulation of extracellular matrix

FIGURE 8. Specificity of the N3ECD antibodies in immunoelectron microscopy staining. **(A–D)** A1-1 antibody immunogold particle reactivity is almost exclusively within a GOM deposit around a VSMC **(A)**, but there is no labeling observed in GOM deposits in negative staining controls **(B)**. There is also no SMA **(C)** or collagen IV **(D)** immunoreactivity within GOM deposits. Black arrows in **(A)**, **(C)**, and **(D)** denote GOM deposits of different sizes; white arrows in **(A)** show GOM deposits with immunogold N3ECD fragments. White arrows denote immunogold particles labeled with anti-SMA **(C)** and anti-collagen IV **(D)** that are not localized within the GOM deposits (black arrows) but only in the respective vascular components. **(E, F)** Anti-ubiquitin immunostaining with 5-nm-gold particles of a vessel wall with GOM in apposition to a VSMC plasma membrane. Higher magnification **(F)** shows the area delineated in **(E)**. The GOM (solid arrow) shows no positive staining for ubiquitin, whereas small clusters of gold spheres are seen within the VSMC (open arrows). L, lumen; N, nucleus. Scale bars = **(A, B, D, E)** 1 μm; **(C)** 350 nm; **(F)** 500 nm.

proteins, which would thicken and stiffen the arterial wall (43–45), could reduce vascular tone and impede the clearance of proteins via the perivascular drainage pathway, thereby resulting in their accumulation within vessel wall, with subsequent damage to the vessel wall and then surrounding tissues (42, 46). Although there is no evidence for direct VSMC toxicity, GOM deposits may themselves reduce vascular functions by their sheer mass that obstructs ISF drainage and exacerbates perivascular damage (Fig. 9). Such mechanical obstruction of the lymphatic drainage system may cause widened perivascular spaces that might be improved by removal of the underlying cause (47). The impairment of perivascular movement of GOM deposits also relates to our observations on the intractable relationships between blood-brain barrier damage, vessel wall thickening, and perivascular space enlargement (5, 21, 48). Similar to the scenario in AD, it would be relevant to examine cervical lymph nodes, where ISF drains into via perivascular drainage pathways to be filtered and GOM could further activate the immune system (40).

A few other limitations in the current study need to be considered. We used autopsy samples for the EM study, and antemortem and postmortem factors impacted the integrity of the brain tissue used. The vascular morphology was reasonably preserved, but many of the cell organelles were destroyed, which sometimes made it difficult to identify the intracellular structures associated with the immunogold EM staining. Thus, well-preserved and properly fixed brain biopsies would be necessary to arrive at more definitive conclusions. Second, although the specificities of N3ECD antibodies and the identical staining pattern among CADASIL cases were confirmed by light microscopy and at the EM level, our data could have been strengthened through the use of scanning EM investigation (although it is extremely labor intensive and can be fraught with more artifacts than transmission EM). Further studies using morphologically better preserved tissue, either from humans or transgenic mice, would confirm the above findings of extracellular mobilization and fate of N3ECD-GOM complexes.

In summary, we detected N3ECD peptides within GOM deposits adjacent to basement membranes of arteries, arterioles, and capillaries in CADASIL patients. Some EM immunoreactivity was found associated with membranous cytoplasmic structures in VSMCs and vesicular inclusions in granular perivascular cells within the meninges.

ACKNOWLEDGMENTS

The authors thank the patients, families, and clinical house staff for their cooperation in the investigation of this study. The authors also thank Janet Slade for excellent technical assistance and Dr. Keikichi Takahashi (NCGG, Obu City, Japan) for making the antibodies to NOTCH3 freely available for use. The authors are indebted to Professor Roy Weller (Southampton, UK) for fruitful discussions and scrutinizing the images.

REFERENCES

1. Chabriat H, Joutel A, Dichgans M, et al. CADASIL. Lancet Neurol 2009; 8:643–53
2. Miao Q, Paloneva T, Tuominen S, et al. Fibrosis and stenosis of the long penetrating cerebral arteries: The cause of the white matter pathology in cerebral autosomal dominant arteriopathy with subcortical infarcts and leukoencephalopathy. Brain Pathol 2004;14:358–64
3. Kalimo H, Ruchoux M-M, Viitanen M, et al. CADASIL: A common form of hereditary arteriopathy causing brain infarcts. Brain Pathol 2002; 12:350–59
4. Ruchoux M-M, Guerouaou D, Vandenhaute B, et al. Systemic vascular smooth muscle cell impairment in cerebral autosomal dominant arteriopathy with subcortical infarcts and leukoencephalopathy. Acta Neuropathol 1995;89:500–12
5. Ruchoux M-M, Maurage C-A. Endothelial changes in muscle and skin biopsies in patients with CADASIL. Neuropathol Appl Neurobiol 1998; 24:60–65
6. Tikka S, Mykknen K, Ruchoux M-M, et al. Congruence between NOTCH3 mutations and GOM in 131 CADASIL patients. Brain 2009; 132:933–39
7. Yamamoto Y, Craggs L, Baumann M, et al. Molecular genetics and pathology of hereditary small vessel diseases of the brain. Neuropathol Appl Neurobiol 2011;37:94–113
8. Maclean AV, Woods R, Alderson LM, et al. Spontaneous lobar haemorrhage in CADASIL. J Neurol Neurosurg Psychiatry 2005;76: 456–57
9. Low WC, Junna M, Börjesson-Hanson A, et al. Hereditary multi-infarct dementia of the Swedish type is a novel disorder different from NOTCH3 causing CADASIL. Brain 2007;130:357–67
10. Lewandowska E, Leszczyńska A, Wierzba-Bobrowicz T, et al. Ultrastructural picture of blood vessels in muscle and skin biopsy in CADASIL. Folia Neuropathol 2007;44:265–73
11. Lewandowska E, Szpak G, Wierzba-Bobrowicz T, et al. Capillary vessel wall in CADASIL angiopathy. Folia Neuropathol 2010;48:104–15
12. Low WC, Santa Y, Takahashi K, et al. CADASIL-causing mutations do not alter Notch3 receptor processing and activation. Neuroreport 2006; 17:945–49
13. Joutel A, Andreux F, Gaulis S, et al. The ectodomain of the Notch3 receptor accumulates within the cerebrovasculature of CADASIL patients. J Clin Invest 2000;105:597–605
14. Ishiko A, Shimizu A, Nagata E, et al. Notch3 ectodomain is a major component of granular osmiophilic material (GOM) in CADASIL. Acta Neuropathol 2006;112:333–39
15. Opherk C, Duering M, Peters N, et al. CADASIL mutations enhance spontaneous multimerization of NOTCH3. Hum Mol Genet 2009;18: 2761–67
16. Duering M, Karpinska A, Rosner S, et al. Co-aggregate formation of CADASIL-mutant NOTCH3: A single-particle analysis. Hum Mol Genet 2011;20:3256–65
17. Weller RO, Djuanda E, Yow H-Y, et al. Lymphatic drainage of the brain and the pathophysiology of neurological disease. Acta Neuropathol 2009; 117:1–14
18. Takahashi K, Adachi K, Yoshizaki K, et al. Mutations in NOTCH3 cause the formation and retention of aggregates in the endoplasmic reticulum, leading to impaired cell proliferation. Hum Mol Genet 2010;19:79–89
19. Deramecourt V, Slade JY, Oakley AE, et al. Staging and natural history of cerebrovascular pathology in dementia. Neurology 2012;78:1043–50
20. Ihara M, Polvikoski TM, Hall R, et al. Quantification of myelin loss in frontal lobe white matter in vascular dementia, Alzheimer's disease, and dementia with Lewy bodies. Acta Neuropathol 2010;119:579–89
21. Yamamoto Y, Ihara M, Tham C, et al. Neuropathological correlates of temporal pole white matter hyperintensities in CADASIL. Stroke 2009; 40:2004–11
22. Narayan SK, Gorman G, Kalaria RN, et al. The minimum prevalence of CADASIL in north east England. Neurology 2012;78:1025–27
23. Kalaria RN, Kenny RA, Ballard CG, et al. Towards defining the neuropathological substrates of vascular dementia. J Neurol Sci 2004;226: 75–80
24. Montine TJ, Phelps CH, Beach TG, et al. National Institute on Aging-Alzheimer's Association guidelines for the neuropathologic assessment of Alzheimer's disease: A practical approach. Acta Neuropathol 2011;123:1–11
25. McKeith IG, Dickson DW, Lowe J, et al. Diagnosis and management of dementia with Lewy bodies: Third report of the DLB Consortium. Neurology 2005;65:1863–72

26. Craggs LJ, Hagel C, Kuhlenbaeumer G, et al. Quantitative vascular pathology and phenotyping familial and sporadic cerebral small vessel diseases. Brain Pathol 2013 Feb 6. [Epub ahead of print] doi: 10.1111/bpa.12041
27. Premkumar DR, Cohen DL, Hedera P, et al. Apolipoprotein E–epsilon4 alleles in cerebral amyloid angiopathy and cerebrovascular pathology associated with Alzheimer's disease. Am J Pathol 1996;148:2083–95
28. Dziewulska D, Lewandowska E. Pericytes as a new target for pathological processes in CADASIL. Neuropathology 2012;32:515–21
29. Rauen T, Raffetseder U, Frye BC, et al. YB-1 acts as a ligand for notch-3 receptors and modulates receptor activation. J Biol Chem 2009;284: 26928–40
30. Arboleda-Velasquez JF, Martinez MC, Donahue CP, et al. CADASIL mutations impair Notch3 glycosylation by Fringe. Hum Mol Genet 2005; 14:1631–39
31. Dziewulska D, Rafalowska J. Is the increased expression of ubiquitin in CADASIL syndrome a manifestation of aberrant endocytosis in the vascular smooth muscle cells? J Clin Neurosci 2008;15:535–40
32. Ruchoux MM, Brulin P, Limol S, et al. Transgenic mice expressing mutant Notch3 develop vascular alterations characteristic of cerebral autosomal dominant arteriopathy with subcortical infarcts and leukoencephalopathy. Am J Pathol 2003;162:329–42
33. Arboleda-Velasquez JF, Manent J, Lee JH, et al. Hypomorphic Notch 3 alleles link Notch signaling to ischemic cerebral small-vessel disease. Proc Natl Acad Sci U S A 2011;108:E128–35
34. Karlström H, Beatus P, Dannaeus K, et al. A CADASIL-mutated Notch 3 receptor exhibits impaired intracellular trafficking and maturation but normal ligand-induced signaling. Proc Natl Acad Sci USA 2002;99: 17119–24
35. Woollard HH. Vital staining of the leptomeninges. J Anat 1924;58:89–100
36. Wu Z, Zhang J, Nakanishi H. Leptomeningeal cells activate microglia and astrocytes to induce IL-10 production by releasing proinflammatory cytokines during systemic inflammation. J Neuroimmunol 2005;167: 90–98
37. Nakanishi H, Wu Z. Microglia-aging: Roles of microglial lysosome- and mitochondria-derived reactive oxygen species in brain aging. Behav Brain Res 2009;201:1–7
38. Thomas WE. Brain macrophages: On the role of pericytes and perivascular cells. Brain Res Brain Res Rev 1999;31:42–57
39. Armulik A, Genove G, Mae M, et al. Pericytes regulate the blood-brain barrier. Nature 2010;468:557–61
40. Unlu M, de Lange RP, de Silva R, et al. Detection of complement factor B in the cerebrospinal fluid of patients with cerebral autosomal dominant arteriopathy with subcortical infarcts and leukoencephalopathy disease using two-dimensional gel electrophoresis and mass spectrometry. Neurosci Lett 2000;282:149–52
41. Salminen A, Ojala J, Kauppinen A, et al. Inflammation in Alzheimer's disease: Amyloid-β oligomers trigger innate immunity defence via pattern recognition receptors. Prog Neurobiol 2009;87:181–94
42. Weller RO, Subash M, Preston SD, et al. Perivascular drainage of amyloid-beta peptides from the brain and its failure in cerebral amyloid angiopathy and Alzheimer's disease. Brain Pathol 2008;18:253–66
43. Lacombe P, Oligo C, Domenga V, et al. Impaired cerebral vasoreactivity in a transgenic mouse model of cerebral autosomal dominant arteriopathy with subcortical infarcts and leukoencephalopathy arteriopathy. Stroke 2005;36:1053–58
44. Hussain MB, Singhal S, Markus HS, et al. Abnormal vasoconstrictor responses to angiotensin II and noradrenaline in isolated small arteries from patients with Cerebral Autosomal Dominant Arteriopathy with Subcortical Infarcts and Leukoencephalopathy (CADASIL). Stroke 2004;35:853–58
45. Dubroca C, Lacombe P, Domenga V, et al. Impaired vascular mechanotransduction in a transgenic mouse model of CADASIL arteriopathy. Stroke 2005;36:113–17
46. Carare RO, Bernardes-Silva M, Newman TA, et al. Solutes, but not cells, drain from the brain parenchyma along basement membranes of capillaries and arteries: Significance for cerebral amyloid angiopathy and neuroimmunology. Neuropathol Appl Neurobiol 2008;34:131–44
47. Cerase A, Venturi C, Rubenni E, et al. Complete regression of a temporal stem dilated perivascular space following resection of a pituitary nonfunctioning macroadenoma. AJNR Am J Neuroradiol 2009;30:E4–E5
48. Giwa MO, Williams J, Elderfield K, et al. Neuropathologic evidence of endothelial changes in cerebral small vessel disease. Neurology 2011;78: 167–74

